Electronic Supplementary Information

Sites-exposed Ti_3C_2 MXene anchored in N-defect g-C_3N_4 heterostructure nanosheets for efficient photocatalytic N_2 fixation

Cong Sun, Zhiqiang Chen, Jian Cui, Kang Li, Hongxia Qu, Huifang Xie, Qin Zhong*

School of Chemical Engineering, Nanjing University of Science and Technology, Nanjing, Jiangsu 210094, PR China.

Corresponding authors: E-mail: qhx@mail.njust.edu.cn; Tel: +86-2584315517; fax: +86-2584315517

Preparation of Ti_3C_2 nanosheets

Preparation of Ti_3C_2: Ti_3AlC_2 powders (particle size < 75 μ m, i.e., 200 mesh; purity > 98 wt %) were purchased from Nanjing Mission new Materials Co. Ltd. Through selective etching of Al layer from Ti_3AlC_2, stacked Ti_3C_2 powder can be obtained. Typically, Ti_3AlC_2 powders was immersed in 50 wt % HF solution (Aladdin Bio-Chem Technology Co, LTD.) with a weight ratio of 1 g Ti_3AlC_2 per 15 mL HF solution for 24 h with magnetically stirring at room temperature. The resulting suspension was washed by deionized water for three times and centrifuged to remove the impurities until the pH of the supernatant reached 6-7. The obtained Ti_3C_2 powders were dried at vacuum oven for 6 h.

Exfoliation of Ti_3C_2: The stacked Ti_3C_2 powders were exfoliated to obtain ultrathin nanosheets. Dimethyl sulfoxide (DMSO, Aladdin Bio-Chem Technology Co, LTD) was selected to enhance the delamination process. In this case, 1 g of Multilayer Ti_3C_2 was added into 15 ml DMSO with magnetically stirring for 24 h at room temperature. The mixture was centrifuged (4200 rpm, 10 minutes) to obtain the intercalated Multilayer Ti_3C_2 powders. And then the intercalated powders were washed by deionized water for three times to remove the residue DMSO. After that, the residue was dispersed in deaerated water in a weight ratio of 10:1 (Ti_3C_2 to water). Afterward, in order to exfoliate the Ti_3C_2 into 2D nanosheets, sonication was carried out in flowing N_2 for 8 hours, and then the suspension was centrifuged with 10000 rpm for 10 min to remove the unexfoliated Ti_3C_2, and the supernatant contains the Ti_3C_2 nanosheets (1 mg ml^{-1}).

Preparation of bulk g-C_3N_4

Synthesis of bulk g-C_3N_4: g-C_3N_4 was prepared by melamine pyrolysis according to a standard literature method. Briefly, 3 g of melamine was calcined at 550 ℃ in a muffle furnace for 4 h using a heating rate of 2 ℃/min.

The detection of ammonia nitrogen

The concentration of produced ammonia was detected through the colorimetric method using Nessler's reagent (determined by absorbance at 425 nm). In a typical procedure, 2ml of the reaction solution after centrifuging at 4200 rpm for 10 min was transferred into a 20 ml colorimeter tube and diluted with DI water to 5 mL, Then, 100 μL of the potassium sodium tartrate solution was added to the sample tube. After adequate blending, 150 μL of Nessler's reagent was added and mixed for ageing 10 min, (the same ratio and method when drawing the standard curve), and then measured by the UV-vis spectrometer. The average of the detected absorbance for three times was the absorbance of the produced ammonia. Fig. S22 shows ammonia nitrogen standard curve for calculating the ammonia concentration from the absorbance.

Photocatalytic H_2 evolution.

Photocatalytic H_2 evolution was taken out in a glass-closed gas circulation system (Beijing Perfectlight Technology Co., Ltd.) with an external-irradiation pyrex glass reaction cell (Fig. S1a). The reaction temperature was precisely controlled at 279 K by circulation of cooling water. 50 mg photocatalysts were directly added into the mixed solution of 40 mL deionized water and 10 mL methanol. A 300 W Xe-lamp with a UV-cut filter (> 420 nm) was used as visible light source, the irradiation area was 30.2 cm^2. Prior to testing, the reactor was completely evacuated at least for 30 min to remove air. The gas product was analyzed every 20 min by an on-line gas chromatograph (GC7806, TCD, molecular sieve 5 Å, Ar carrier).The Photocatalytic H_2 evolution under N_2 atmosphere was carried out through bubbling N_2 for 30min after accomplishing evacuating.

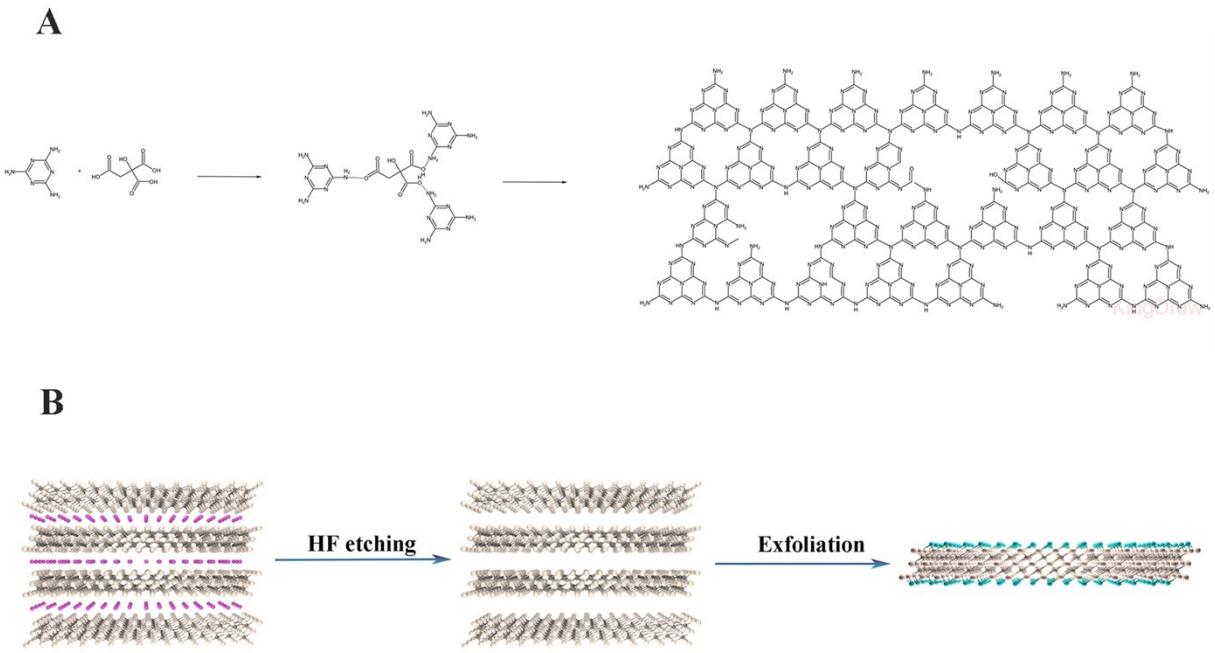

Fig. S1 Schematic illustration of the preparation process for (A) CN and (B) Ti_3C_2 nanosheets.

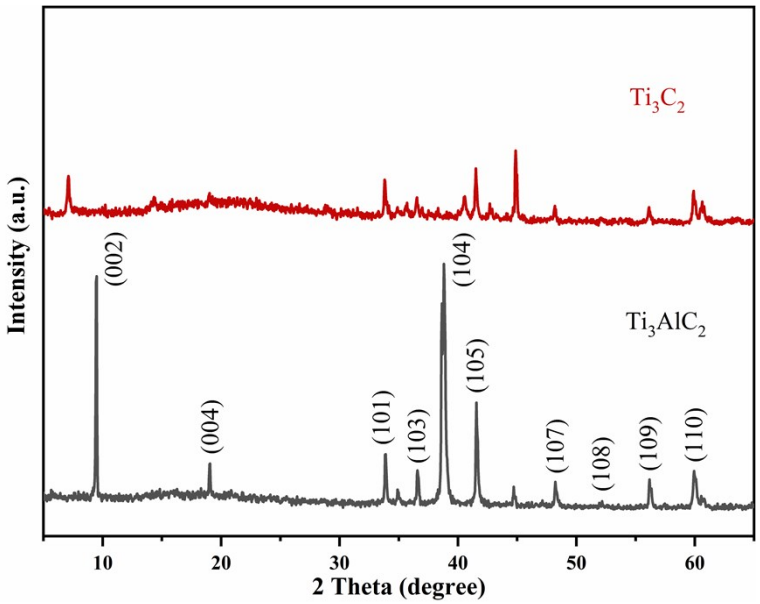

Fig. S2 The XRD patterns of Ti_3AlC_2 and Ti_3C_2

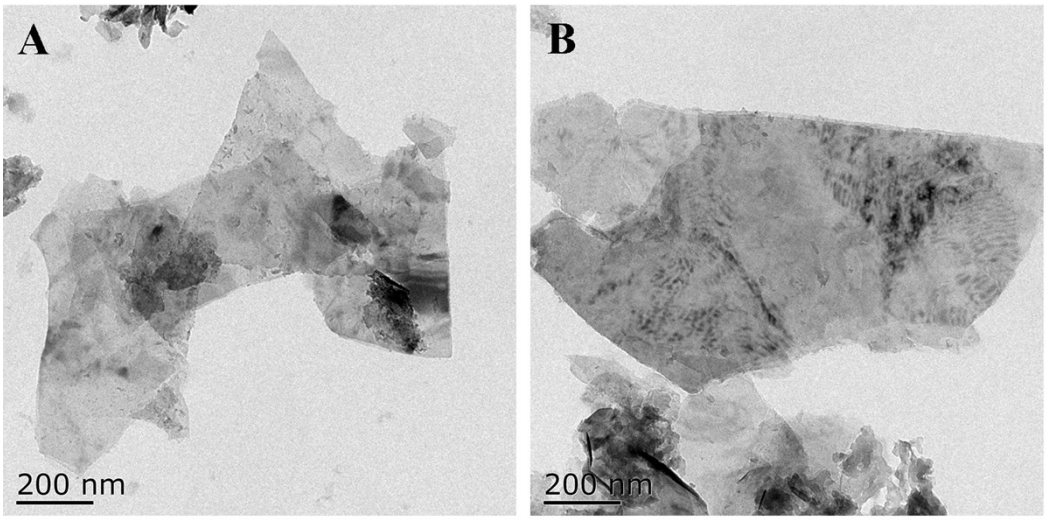

Fig. S3 TEM images of Ti_3C_2.

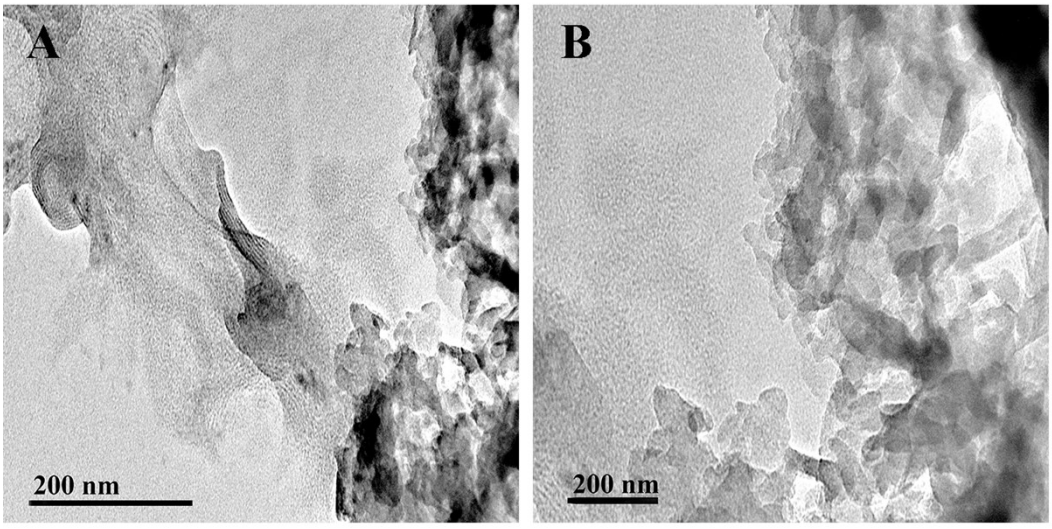

Fig. S4 TEM images of g-C_3N_4.

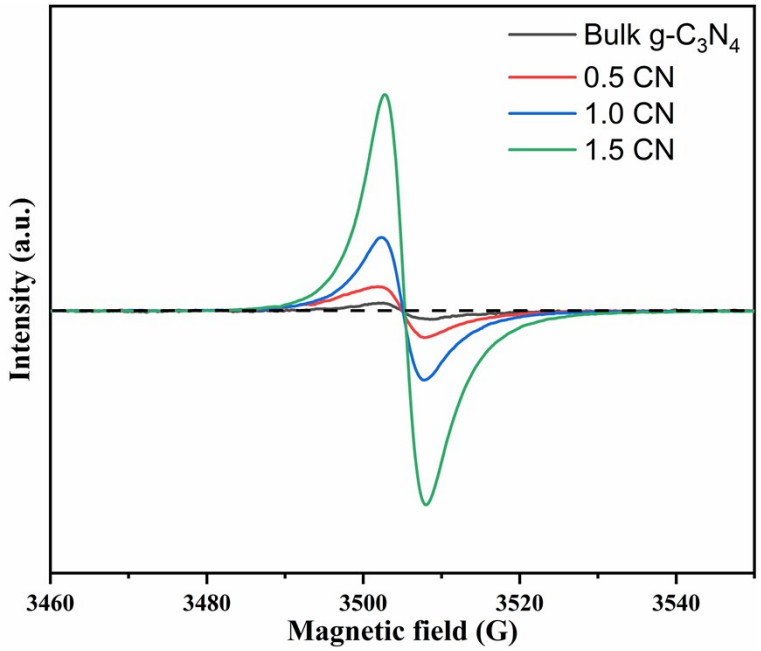

Fig. S5 EPR spectra of bulk g-C_3N_4 and CN.

The 0.5, 1.0 and 1.5 CN was prepared according to the experimental section 2.1 with different citric acid mass of 0.095, 0.190 and 0.285 g per 3 g melamine. The EPR signals for all samples correspond to the same type of unpaired electrons trapped by N-defects. It is evident that citric acid-assist thermal polymerization can induce abundant N-defects in bulk g-C_3N_4, and the concentration of N-defect is positively correlated with the content of citric acid.

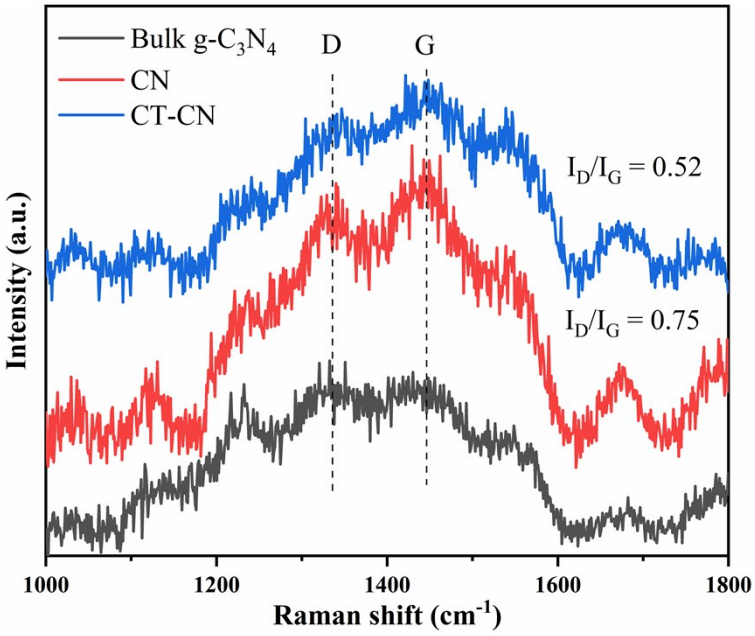

Fig. S6 Raman spectra of bulk g-C_3N_4, CN and CT-CN.

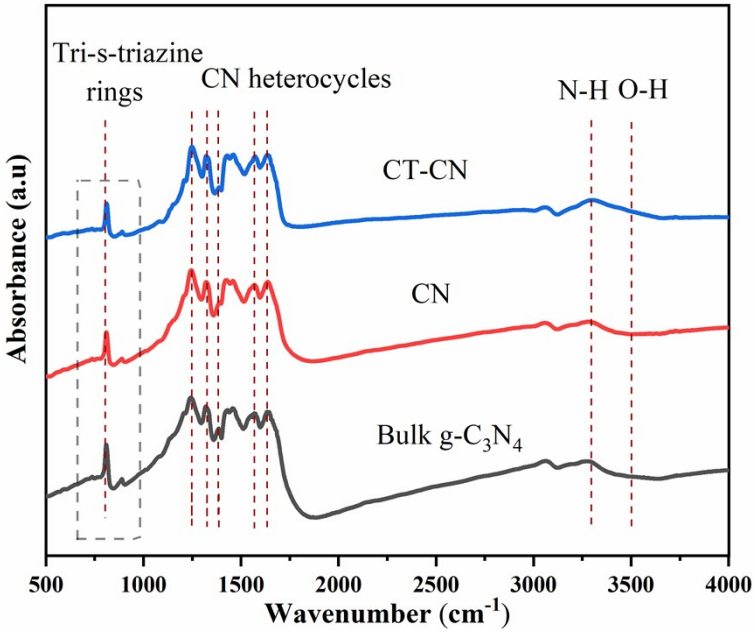

Fig. S7 FT-IR spectra of bulk g-C_3N_4, CN and CT-CN.

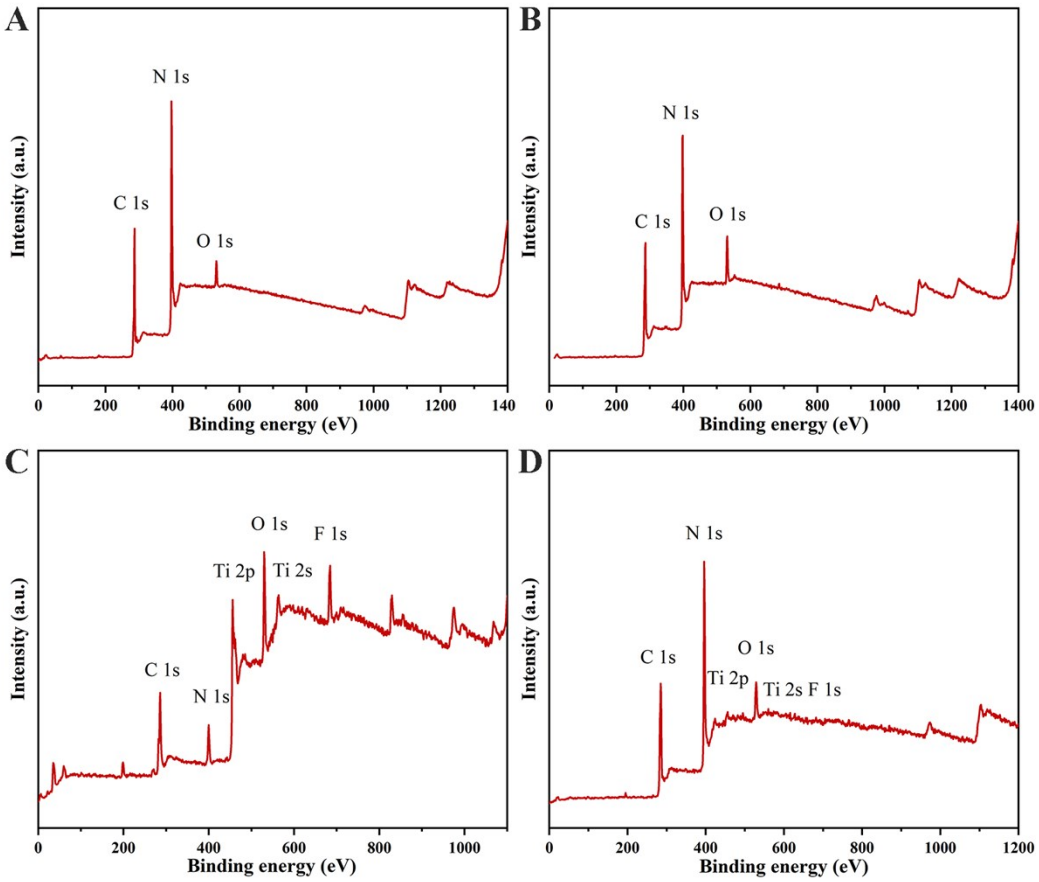

Fig. S8 XPS survey spectra of (A) bulk g-C_3N_4, (B) CN, (C) Ti_3C_2 and (D) CT-CN.

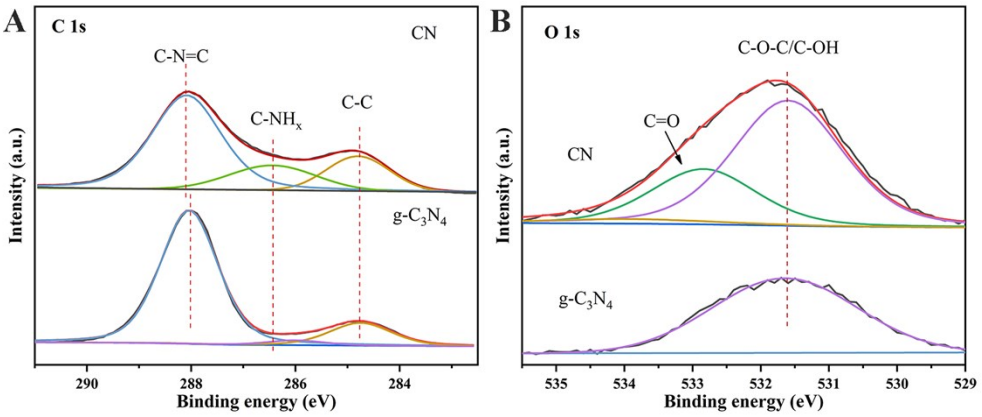

Fig. S9 (A) C 1s and (B) O 1s XPS spectra of Ti_3C_2 and CN

As shown in Fig. S9A, the peak of C-N=C for CN is obviously weaker in comparison with g-C_3N_4, resulting from the damaged triazine units caused by the introduced N-defects. Meanwhile, a greatly increased intensity of the peak (C-NHx on the edges of heptazine units) is observed, implying numerous amino groups are produced on the N-defects. Fig. S9B exhibits O 1s XPS spectra of g-C_3N_4 and CN. the enhanced C-OH/C-O-C peak and a new C=O peak indicate Oxygen-containing groups are introduced in CN.

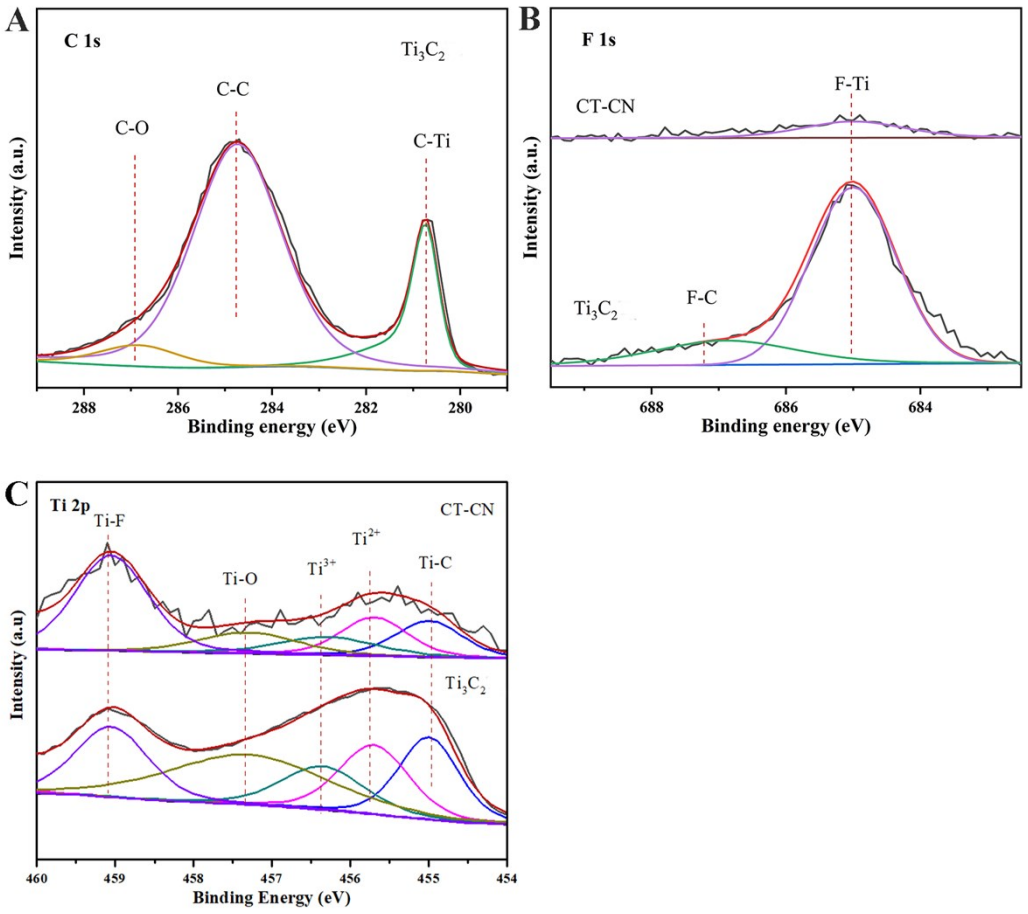

Fig. S10 (A) C 1s, (B) F 1s and (C) Ti 2p XPS spectra.

The C 1s XPS spectra of Ti_3C_2 (Fig. S10A) can be deconvoluted into three peaks at 280.7 eV, 284.8 eV and 286.9 eV, corresponding to the C-Ti on the skelecton, graphitic C-C and C-O originated from the selective dissolution of Ti during etching. For F 1s (Fig. S10B), a terminal F-Ti at 685 eV and F-C at 687.2 eV are observed. As shown in Fig. S10C, the Ti 2p XPS spectra are divided into five peaks at 451.7, 452.4, 453.0, 454.0 and 455.8 eV, corresponding to Ti-C on the skelecton, Ti^{2+} as well as Ti^{3+} on the edge or defect of Ti_3C_2, Ti-O and Ti-F on the terminal groups. The CT-CN exhibits the same peak as that of Ti_3C_2.

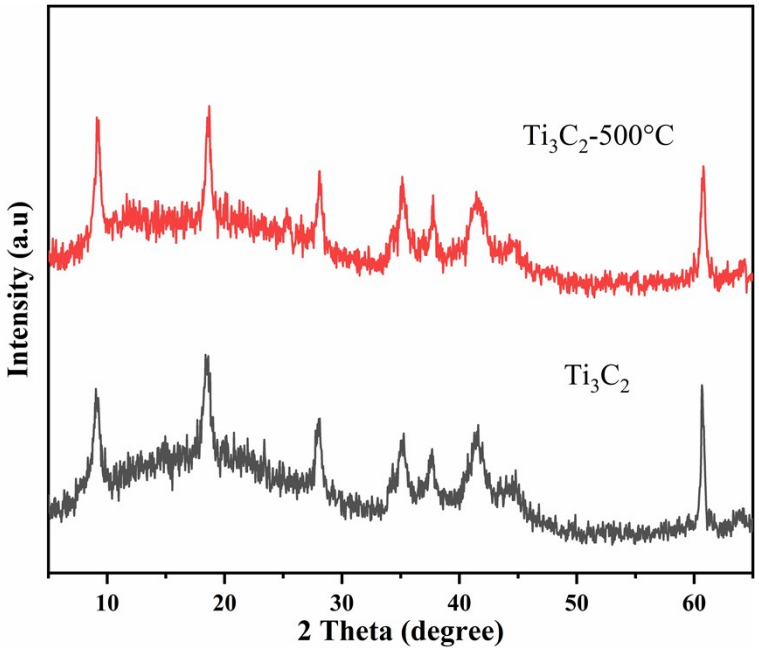

Fig. S11 The XRD patterns of Ti_3C_2 and Ti_3C_2 after treated in 300℃.

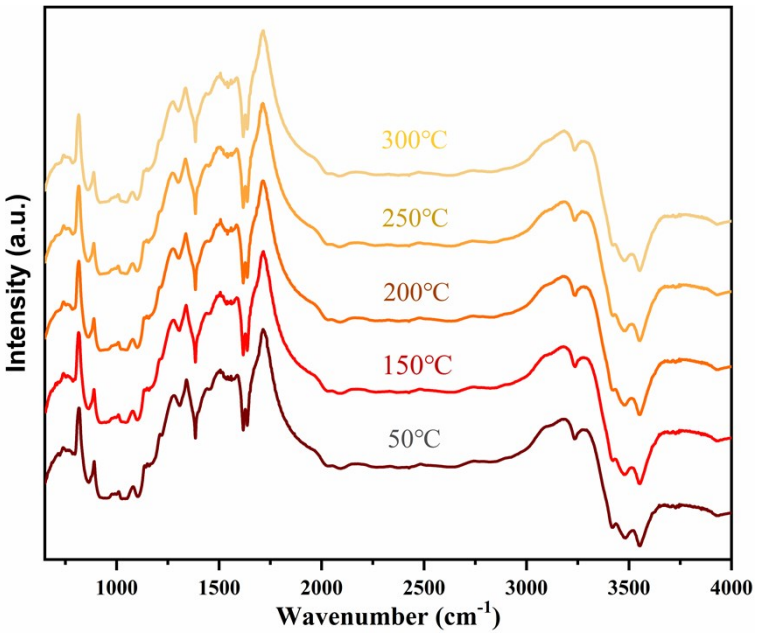

Fig. S12 In situ DRFTIRS spectra of CT-CN treated in an increasing temperature from 50 ℃ to 300 ℃

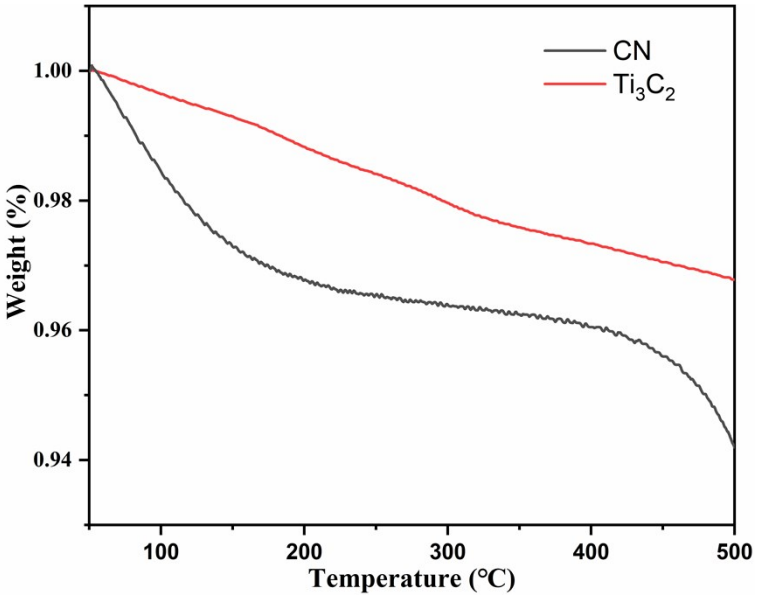

Fig. S13 The TG analysis of CN and Ti_3C_2.

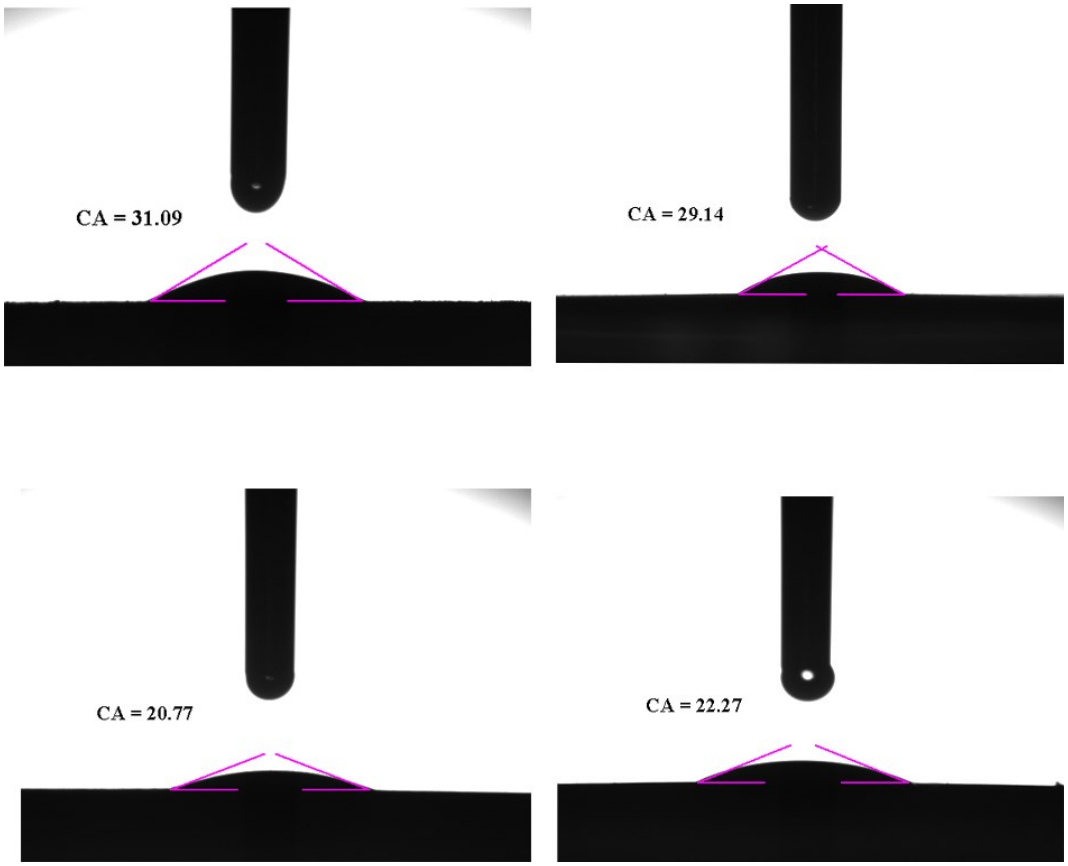

Fig. S14 The contact Angle tests of bulk g-C_3N_4, CN, CT-CN and CT-CN treated in 300 ℃..

As shown in Fig. S11, Ti_3C_2 exhibits no change in the XRD patterns after treated in 300 ℃, indicating a heating treatment in such temperature does not affect the structure of Ti_3C_2. In situ DRFTIRS spectra (Fig. S12) records the chemical structure of CT-CN during the heating treatment process. Obviously, the C_3N_4 triazine structure is maintained after a treatment at 300 ℃. However, the TG (Fig. S13) reveals a continual decline in mass of CN and Ti_3C_2 during the heating process. Combined with the results of the XRD and in situ DRFTIRS, it suggests a loss of surface groups in both CN and Ti_3C_2. Fig. S14 shows the contact Angle test result. The groups obtained by the introduction of N-defects and the combination with Ti_3C_2 result in the great hydrophilia for CT-CN. After treated in 300 ℃, a decrease in contact Angle suggests a reduced hydrophilia due to the loss of hydrophilic groups.

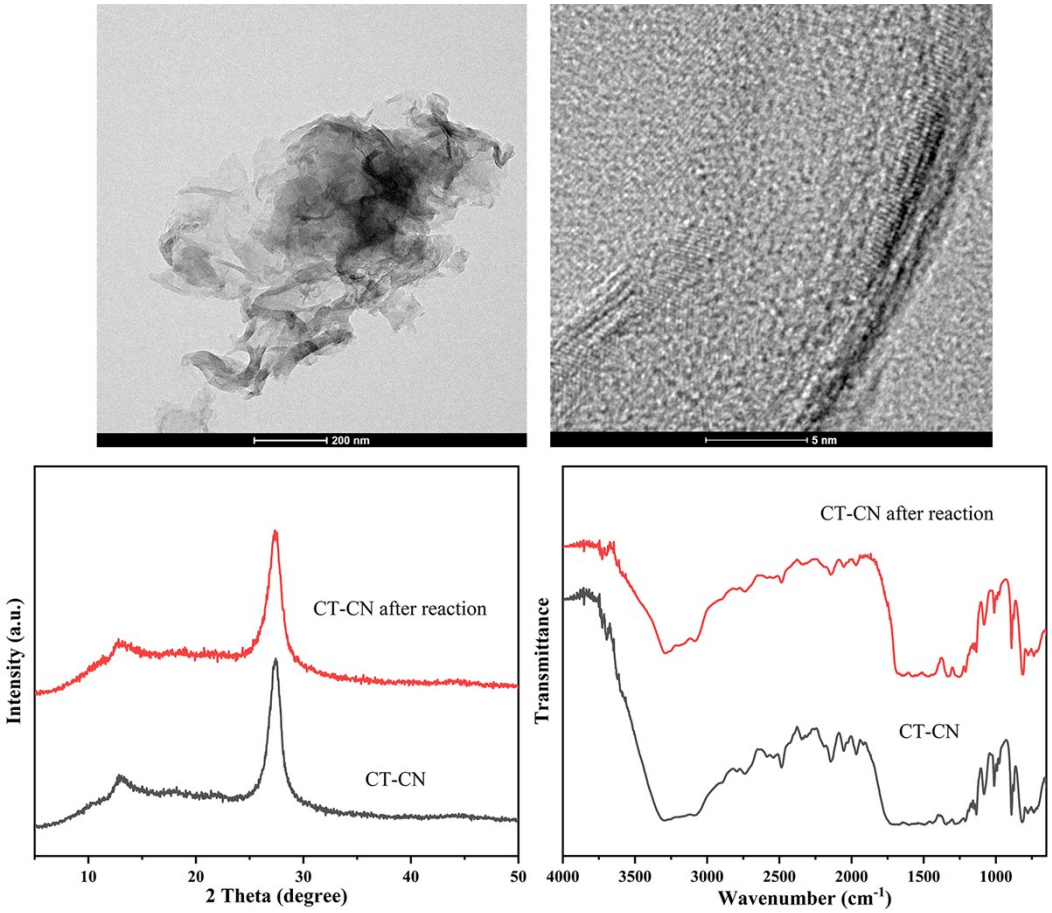

Fig. S15 (A) TEM and (B) HRTEM images of CT-CN after reaction; (C) XRD patterns and (D) FT-IR spectra of CT-CN before and after reaction.

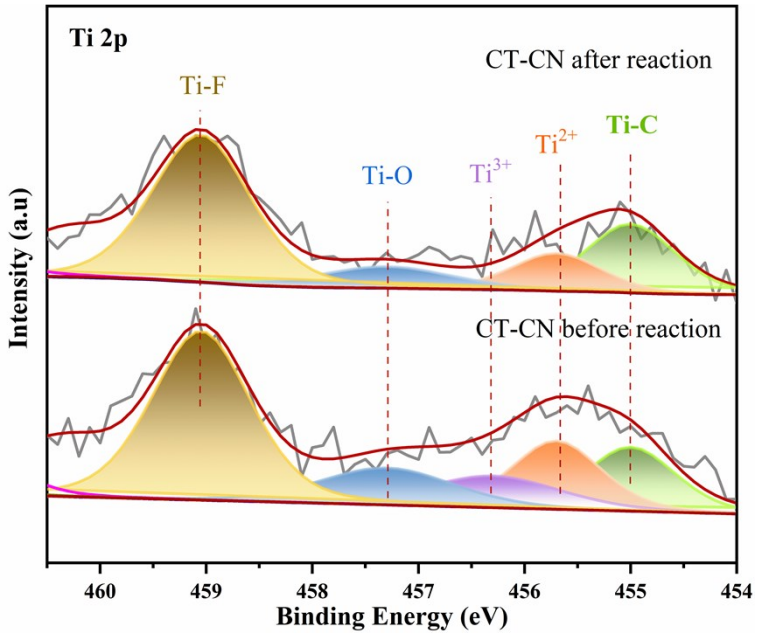

Fig. S16 Ti 2p XPS spectra of CT-CN before reaction and after reaction.

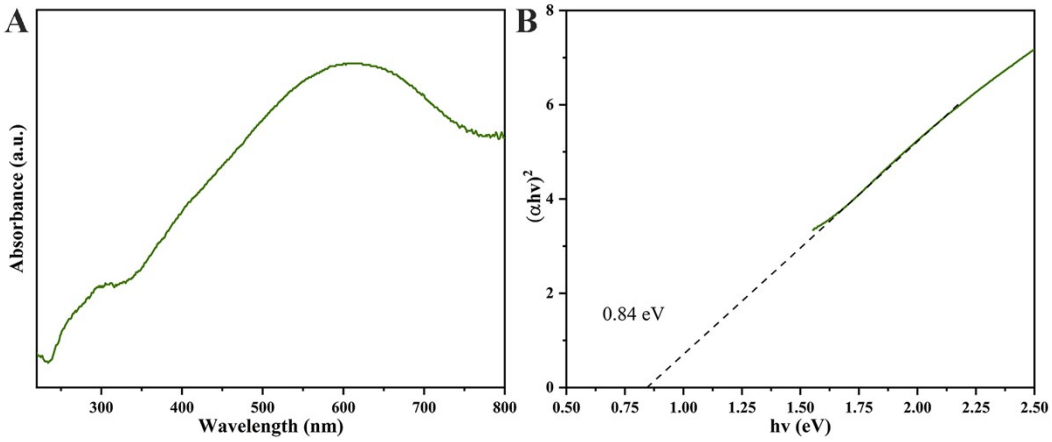

Fig. S17 (A) UV-vis DRS spectrum and (B) plot of transformed Kubelka–Munk function versus photon energy of Ti_3C_2.

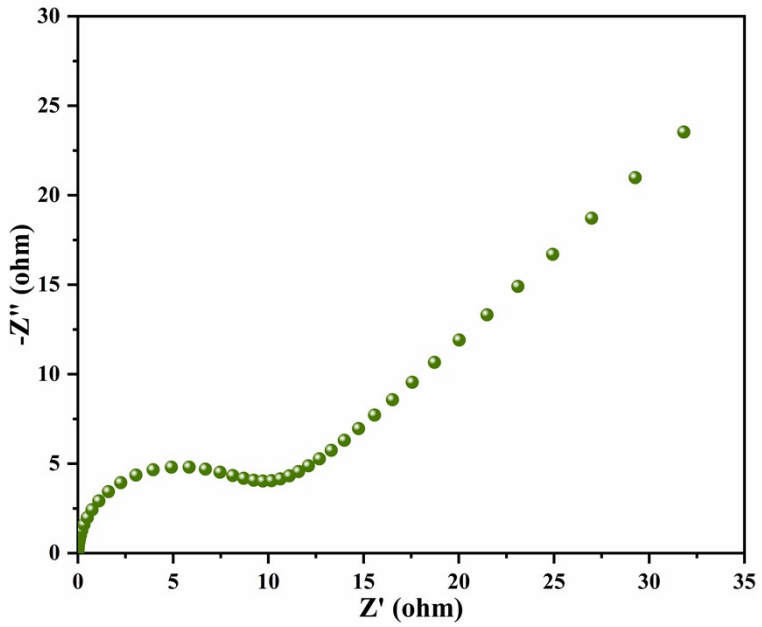

Fig. S18 Electrochemical impedance spectrum of Ti_3C_2.

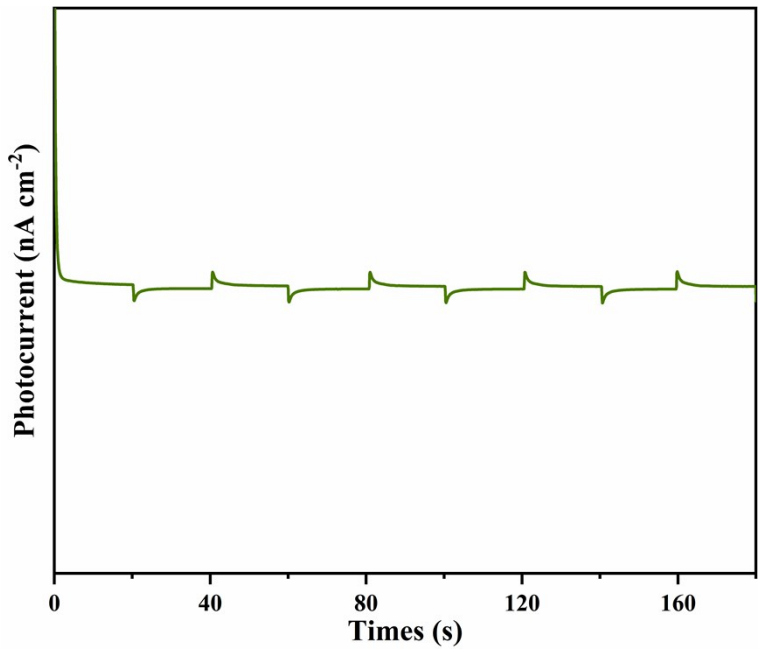

Fig. S19 Transient photocurrent response of Ti_3C_2.

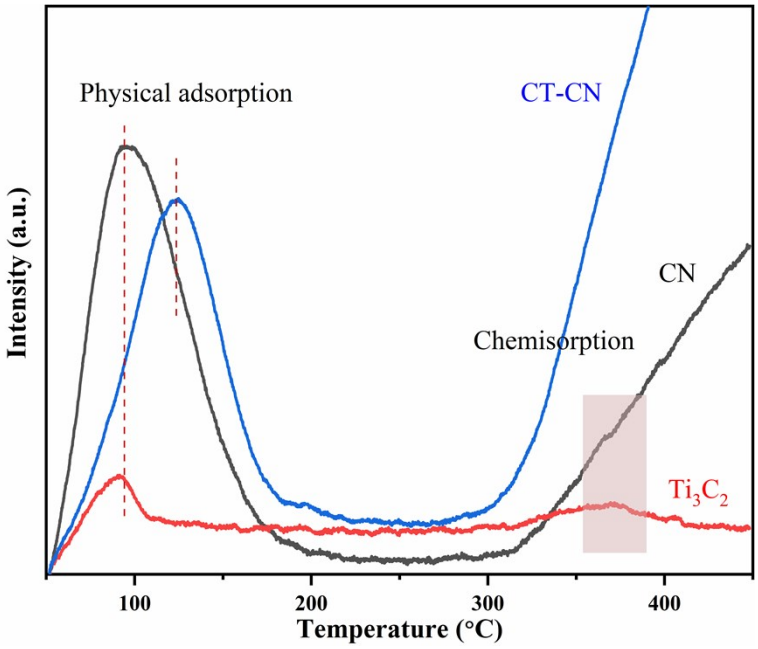

Fig. S20 N_2-TPD of CN, Ti_3C_2 and CT-CN.

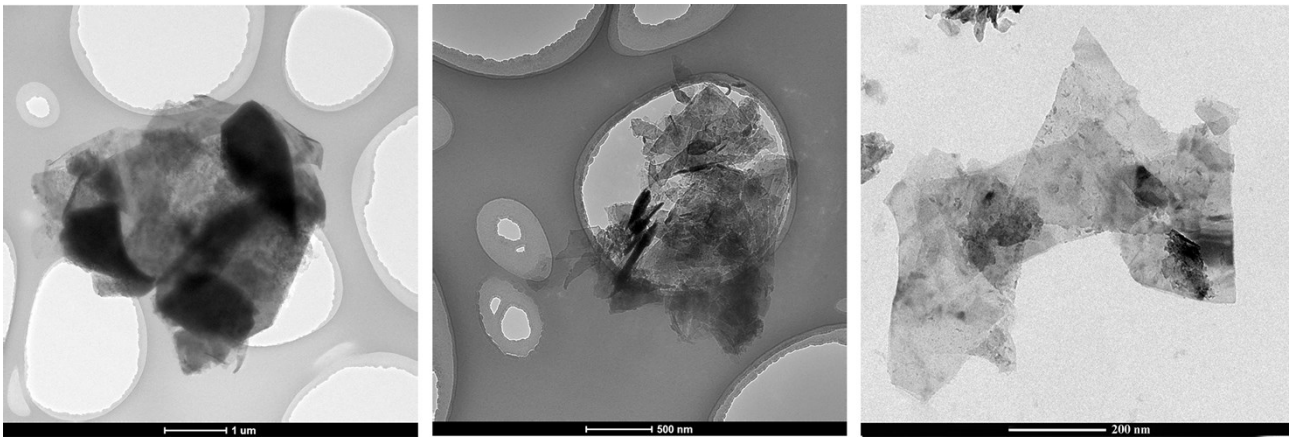

Fig. S21 TEM images of Ti_3C_2 centrifuged at the speed of 0 rpm, 5000 rpm and 10000 rpm.

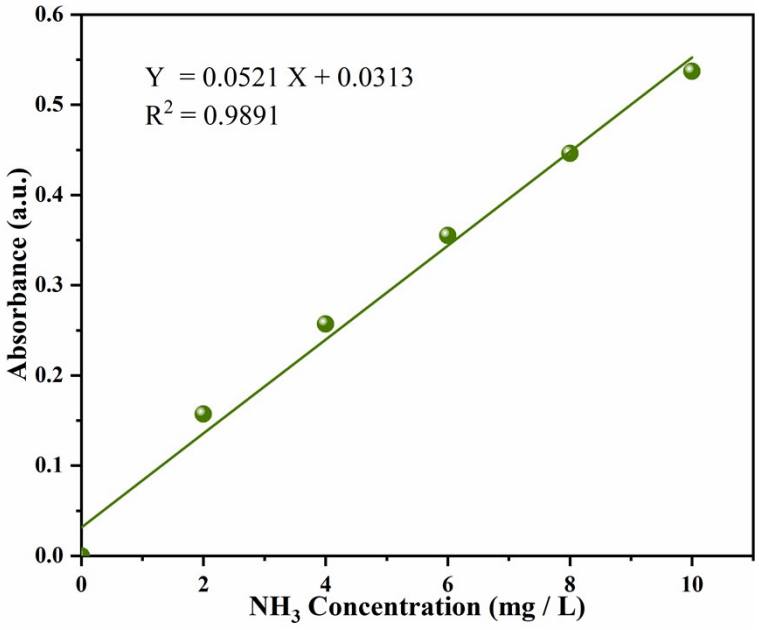

Fig. S22 Ammonia nitrogen standard curve.

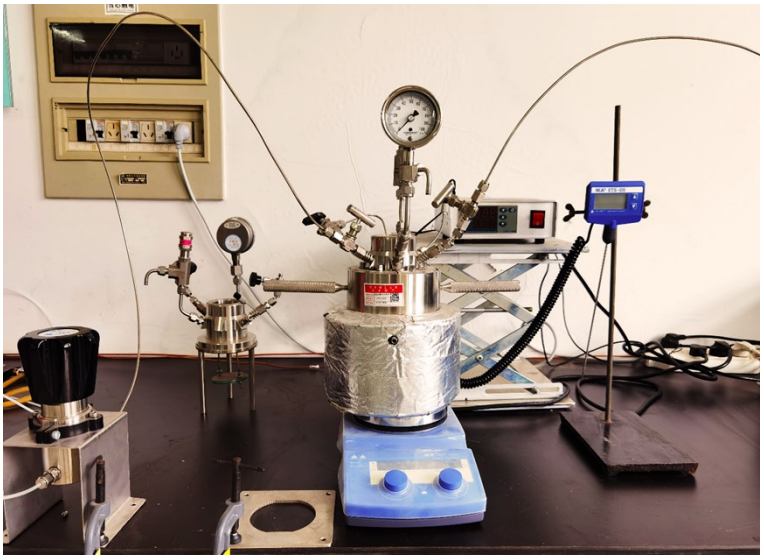

Fig. S23 Photograph of photocatalytic reactor.

Table S1. XPS analysis of C, N in g-C_3N_4 and CN

Sample	C 1s			N 1s			
	Position	Asignment	C/C_{total}	Position	Asignment	N/N_{total}	C/N
g-C_3N_4	284.8	C-C	0.196	398.6	N_{2C}	0.786	0.983
	286.1	C-NH_x	0.087	399.6	N_{3C}	0.163	
	287.7	C=N-C	0.717	400.9	NH_x	0.051	
CN	284.8	C-C	0.167	398.6	N_{2C}	0.621	1.069
	286.4	C-NH_x	0.222	399.5	N_{3C}	0.293	
	288.0	C=N-C	0.611	400.9	NH_x	0.087	

Table S2. Comparison of different reported photocatalysts for photocatalytic N_2 fixation

Photocatalyst	Scavenger	Light Source	NH_3 yield	Ref.
CT-CN	methanol	300 W Xe lamp	5.79 mg h^{-1} g_{cat}^{-1}	This work
Li-3D-GCN	methanol	400–800 nm	2.41 mg h^{-1} g_{cat}^{-1}	S-1
Fe-doped g-C_3N_4	Ethanol	400–800 nm	2.55 mg h^{-1} g_{cat}^{-1}	S-2
Ga_2O_3-DBD/ g-C_3N_4	0.04 mM CH_3OH	500 W Xe lamp	4.78 mg h^{-1} g_{cat}^{-1}	S-3
Single Cu atom modified g-CN	20% CH_3OH	(420~780 nm)	3.16 mg h^{-1} g_{cat}^{-1}	S-4
g-C_3N_4/Fe_2O_3	Methanol	300 W Xe lamp	1.00 mg h^{-1} g_{cat}^{-1}	S-5
TiO_2@C/ g-C_3N_4	Methanol	λ >420 nm	4.25 mg h^{-1} g_{cat}^{-1}	S-6
Fe-EDTA–CNNS	methanol	> 420 nm	2.61 mg h^{-1} g_{cat}^{-1}	S-7

Table S3. XPS analysis of Ti in CT-CN before reaction and CT-CN after reaction.

Sample	Binding energy /eV	Assignment	Ti / Ti_{total}
CT-CN before reaction	451.7	Ti-C	0.152
	452.4	Ti^{2+}	0.163
	453.0	Ti^{3+}	0.114
	454.0	Ti-O	0.132
	455.8	Ti-F	0.440
CT-CN after reaction	451.7	Ti-C	0.228
	452.4	Ti^{2+}	0.126
	453.0	Ti^{3+}	0
	454.0	Ti-O	0.109
	455.8	Ti-F	0.537

References

[S-1] G. Gu, K. Wang, N. Xiong, Z. Li, Z. Fan, S. Hu and X. Zou, *Dalton Trans.*, 2019, **48**, 5083.

[S-2] S. Hu, X. Chen, Q. Li, F. Li, Z. Fan, H. Wang, Y. Wang, B. Zheng and G. Wu, *Appl. Catal. B.*, 2017, 201, 58.

[S-3] S. Cao, N. Zhou, F. Gao, H. Chen and F. Jiang, *Appl. Catal. B.,* 2017, **218**, 600.

[S-4] P. Huang, W. Liu, Z. He, C. Xiao, T. Yao, Y. Zou, C. Wang, Z. Qi, T. Wei,; B. Pan and Sci. *China Chem.*, 2018, **1,** 213.

[S-5] H. Mou, J. Wang, D. Zhang, D. Yu, W. Chen, D. Wang and T. Mu, *J. Mater. Chem. A.*, 2019, **7**, 5719.

[S-6] Q. X. Liu, L. H. Ai and J. Jiang, *J. Mater. Chem. A*., 2018, **6**, 4102.

[S-7] C. Yao, R. Wang, Z. Wang, H. Lei, X. Dong and C. He, *J. Mater. Chem. A*., 2019, **7**, 27547.